PRAMANA
— journal of
physics

Vol. 70, No. 6
June 2008
pp. 1055–1061

Probabilistic signatures of spatiotemporal intermittency in the coupled sine circle map lattice

ZAHERA JABEEN[1] and NEELIMA GUPTE[2,*]
[1]Institute of Mathematical Sciences, CIT Campus, Taramani, Chennai 600 113, India
[2]Department of Physics, Indian Institute of Technology Madras, Chennai 600 036, India
[*]Corresponding author. E-mail: gupte@physics.iitm.ac.in

Abstract. The phase diagram of the coupled sine circle map system exhibits a variety of interesting phenomena including spreading regions with spatiotemporal intermittency, non-spreading regions with spatial intermittency, and coherent structures termed solitons. A spreading to non-spreading transition is seen in the system. A cellular automaton version of the coupled system maps the spreading to non-spreading transition to a transition from a probabilistic to a deterministic cellular automaton. The solitonic sector of the system shows spatiotemporal intermittency with soliton creation, propagation and absorption. A probabilistic cellular automaton mapping is set up for this sector which can identify each one of these phenomena.

Keywords. Coupled map lattice; spatiotemporal intermittency; cellular automata.

PACS Nos 05.45.Ra; 05.45.-a; 05.45.Df; 64.60.Ak

1. Introduction

The coupled sine circle map lattice has been known to model the mode-locking behaviour [1] seen commonly in coupled oscillators, Josephson junction arrays, etc., and is also found to be amenable to analytical studies [2,3]. In addition to mode-locked and synchronised behaviour, the model exhibits a rich variety of phenomena such as spatiotemporal intermittency of the directed percolation class [4,5], spatial intermittency, cluster solutions and regimes with long-lived coherent structures, also known as solitons [6].

The coupled sine circle map lattice is defined on a one-dimensional lattice, and evolves via the equation:

$$x_i^{t+1} = (1-\epsilon) f(x_i^t) + \frac{\epsilon}{2} f(x_{i-1}^t) + \frac{\epsilon}{2} f(x_{i+1}^t) \pmod 1. \tag{1}$$

Here, x_i^t defines the state variable at site i ($i = 1, \ldots, N$, where N is the system size) and time t. The site i at each time step is coupled to its two nearest neighbours $i-1$ and $i+1$ with a coupling strength ϵ. The local map at each site i, $f(x_i^t)$ is the sine circle map defined as $f(x) = x + \Omega - \frac{K}{2\pi}\sin(2\pi x)$, where K denotes

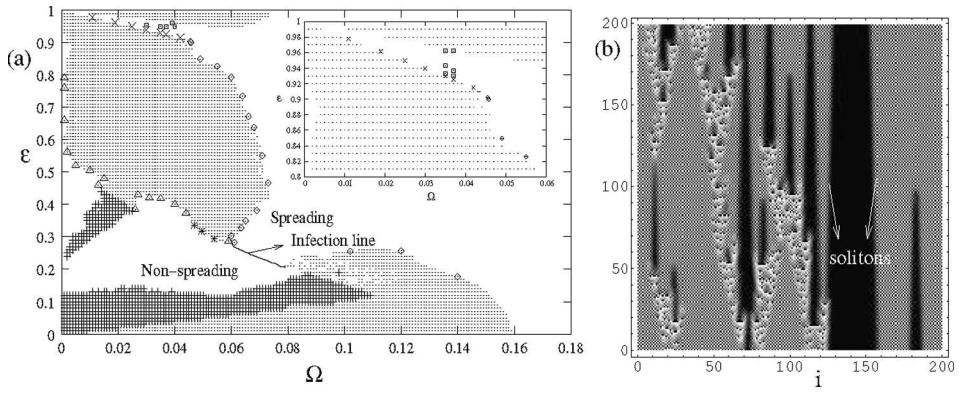

Figure 1. (**a**) The phase diagram obtained for a lattice of size $N = 1000$, after discarding 15,000 transients. Synchronised solutions are seen in the region marked with dots. Spatiotemporal intermittency of the DP class is seen at points marked with diamonds ($\diamond$), and spatial intermittency at points marked with triangles ($\triangle$) and asterisks ($*$). Inset shows a part of the phase diagram where spatiotemporal intermittency with travelling wave laminar states and solitons is seen at points marked with boxes ($\square$). (**b**) The space-time plot of spatiotemporal intermittency with solitons.

the strength of nonlinearity in the map and Ω is the frequency of the map in the absence of nonlinearity.

The phase diagram of the model has been obtained in earlier studies [5] by synchronously updating the coupled sine circle map lattice with random initial conditions, in the parameter region $0 < \Omega \leq \frac{1}{2\pi}$, $0 \leq \epsilon \leq 1$ and at $K = 1.0$. The phase diagram is seen to be organised around the bifurcation boundary of the spatiotemporally synchronised solution as well as a line, called the infection line, that separates the lower half of the parameter space into a spreading and a non-spreading regime (figure 1a). The burst states are capable of infecting their neighbouring laminar states in the spreading regime, whereas they are seen to be non-infectious and localised in the non-spreading regime. Spatiotemporal intermittency contaminated by long-lived travelling coherent structures, also named as solitons, is seen in the upper part of the phase diagram (figure 1a (inset)).

Special behaviour is seen near the bifurcation boundary of the synchronised solutions in these two regimes. In the spreading regime, spatiotemporal intermittency with exponents of the directed percolation (DP) universality class is seen near the bifurcation boundary of the synchronised solutions. This type of intermittency is completely free of coherent structures and a complete set of exponents obtained at the onset of this intermittency matches convincingly with the directed percolation class [5]. In the non-spreading regime, spatial intermittency (SI) with synchronised laminar states and periodic or quasi-periodic bursts are seen near the bifurcation boundary [6]. The scaling exponents for the laminar length distributions in this type of intermittency are seen to be similar to those obtained for spatial intermittency seen in the inhomogeneous logistic map lattice [7].

Further insights into the spreading to non-spreading transition are obtained when the coupled map lattice is mapped onto a cellular automaton [8]. In the spreading regime, including the points where DP behaviour is seen, the probabilities associated with the cellular automaton update rules are seen to lie in the $(0, 1)$ interval. In other words, the update rules obtained in the spreading regime are seen to be probabilistic. In contrast, the probabilities in the entire non-spreading regime are seen to be either zero or one. Thus, the update rules in non-spreading regime are found to be deterministic. Therefore, the cellular automaton mapping of the coupled map lattice shows that the spreading regime can be mapped onto a set of probabilistic cellular automata whereas the entire non-spreading regime can be mapped to a deterministic cellular automaton.

Apart from the spatiotemporal intermittency of the directed percolation class and the spatial intermittency seen in the lower part of the phase diagram, spatiotemporal intermittency with travelling wave laminar states interspersed with turbulent bursts is seen in the upper part of the phase diagram (see inset of figure 1a). This kind of spatiotemporal intermittency contains coherent structures or 'solitons', which spoil the analogy with directed percolation and are responsible for non-universal exponents in this region [6]. In this paper, we show that a cellular automaton can be designed for this type of spatiotemporal intermittency, which successfully picks up signatures of the 'solitons'. We discuss this in the following section.

2. Spatiotemporal intermittency with travelling wave laminar states and solitons

Spatiotemporal intermittency with travelling wave laminar states is seen in the upper part of the phase diagram at points marked with boxes (□) (figure 1a). In this type of intermittency, the lattice relaxes to the absorbing travelling wave laminar state asymptotically. The burst states are turbulent and lie in the interval $(0, 1)$, and can spread through the lattice. Apart from the burst states, coherent structures, which have been called 'solitons', are seen in the travelling wave laminar background. These structures have been marked in the space-time plot of this type of spatiotemporal intermittency in figure 1b. As can be seen from the space-time plot, these solitons are generated from the turbulent burst states. Moreover, both left-moving and right-moving solitons occur in pairs in the lattice and eventually annihilate each other on collision. When these solitons collide, they either die down to the travelling wave laminar state or give rise to turbulent bursts. Therefore, the burst states are created in the lattice either by infection of a laminar site by a neighbouring burst site or by the annihilation of solitons. Regions of synchronised fixed point solutions, $x^\star$ are seen to exist between the left- and right-moving solitons, which perish with the annihilation of the solitons. The coherent structures seen in this type of spatiotemporal intermittency show a strong resemblance to the 'solitons' seen in the Chaté–Manneville coupled map lattice [9], where these solitons were responsible for spoiling the directed percolation behaviour [10,11].

The solitons alter the dynamical behaviour of the system in this regime in several significant ways. They spoil the analogy with DP behaviour by acting as an

Table 1. The laminar length distribution exponent, ζ obtained for different values of the coupling strength, ϵ at $\Omega = 0.035$ in the spatiotemporal intermittency with travelling wave laminar state and solitons regime. The table also shows the scaling exponents associated with the distribution of soliton lifetimes, and the maximum soliton lifetime observed, $T_{\max}$.

$\Omega = 0.035$		Distribution of soliton lifetimes		
ϵ	ζ	Nature	Scaling exponent	$T_{\max}$
0.933	1.53 ± 0.01	Scales with a power-law	1.14	19010
0.943	1.40 ± 0.01	Scales with a power-law	1.35	2481
0.950	1.17 ± 0.01	Scales with a power-law	1.64	794
0.962	1.02 ± 0.01	Peaked distribution with a power-law tail	2.84	305

additional source of turbulent bursts. They also introduce a new time-scale in the system, namely the soliton lifetime, which depends on Ω and ϵ and gives rise to non-universal exponents. This can be seen in table 1 in which the scaling exponents ζ associated with the distribution of laminar lengths $P(l) \sim l^{-\zeta}$, obtained at various values of coupling strengths ϵ for $\Omega = 0.035$ have been shown.

The exponent ζ is seen to vary from 1 to 1.5 for different values of ϵ. The soliton lifetimes also decrease with increase in coupling strength and give rise to two distinct regimes. In regimes of long average soliton lifetimes, the distribution of soliton lifetimes shows a power-law behaviour whereas the distribution shows a peak with a characteristic time-scale (~ 20) in regimes of short soliton lifetimes. These varying average soliton lifetimes influence the extent of spreading in the lattice and therefore lead to varying values for the laminar length distribution exponents [6]. Thus, the creation, propagation, and annihilation of solitons lead to significant changes in the statistical and dynamical behaviour of the system. A cellular automaton mapping for this type of spatiotemporal intermittency can be designed which mimics the dynamics observed in this region [9,12,13], and contains significant signatures of these solitonic processes. We discuss this in the next section.

3. A cellular automaton for spatiotemporal intermittency containing solitons

The cellular automaton is defined on a $(1+1)D$ lattice. There are four states in the solitonic region, the travelling wave laminar state, the burst state, the soliton state, and the fixed point state. Therefore, the variable v_i^t at site i and time t is assigned a value $v_i^t = 0$ if it exists in the travelling wave laminar state, $v_i^t = 1$ for a burst state, $v_i^t = 2$ for a solitonic state, and $v_i^t = 3$ if it exists in the fixed point state, $x^\star$. Since, the probability that the site i at time $t+1$ exists in the state v_i^{t+1}, depends on the states of the sites $i-1, i, i+1$ at time t as defined in the evolution equation (1), the update rules of the cellular automaton are given by the conditional probability $P(v_i^{t+1}|v_{i-1}^t, v_i^t, v_{i+1}^t)$.

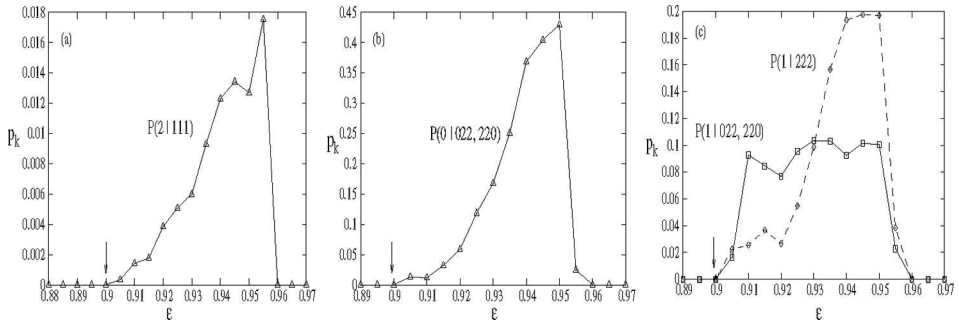

Figure 2. The probabilities (**a**) $P(2|111)$, which indicate the creation of solitons, (**b**) $P(0|022, 220)$ which is the probability of propagation of solitons, and (**c**) $P(1|222)$ and $P(1|022, 220)$, which gives the probability of creation of bursts due to the annihilation of solitons. These probabilities have been obtained for various values of the coupling strengths ϵ at $\Omega = 0.0455$.

For the above defined CA, 4^3 initial states are possible. After considering the four possible final states $v_i^{t+1} = 0, 1, 2, 3$, we can define 4×4^3 update rules of the cellular automaton in this region. However, the number of relevant update rules required to understand the dynamics is much smaller, and can be reduced by (i) using the symmetry between the sites $i-1$ and $i+1$ as defined in the evolution equation, and considering the states $P(v_i^{t+1}|001)$ and $P(v_i^{t+1}|100)$ (say) as equivalent, (ii) eliminating the states which do not exist as neighbours (e.g.: the states $v_i^t = 0$ and $v_i^t = 3$ do not exist as nearest neighbours, as the travelling wave state and the fixed point state are never nearest neighbours). Finally, we reduce the number further by focussing on states which appear more frequently in the system.

The values of these probabilities can be estimated from the evolution of the CML equation (1) starting from random initial conditions. Let N_k be the number of sites i at time t, which along with its neighbours $i-1$ and $i+1$ exist in the kth state at time t. If N_k^0, N_k^1, N_k^2, and N_k^3 be the fraction of N_k sites, which, at time $t+1$, exist in 0 (travelling wave), 1 (burst), 2 (soliton) and 3 (fixed point $x^\star$) states respectively such that $N_k = N_k^0 + N_k^1 + N_k^2 + N_k^3$, then the probability p_k^m is estimated using $p_k^m = N_k^m/N_k$, where $m = 0, 1, 2$, or 3.

As a result, we get the following 17 prominent initial configurations that constitute at least 0.1% of the total dynamics: 000, (001, 100), 010, (011, 110), 101, 111, (002, 200), (022, 220), (112, 211), (122, 221), 222, (331, 133), (311, 113), (332, 233), (322, 223), 232, and 333. Further identification of the most relevant update rules is carried out by concentrating on those configurations which show a higher probability of transition to the final states $v_i^{t+1} = 0, 1, 2$, or 3.

The CA probabilities thus identified contain information about the infective dynamics of the burst states and also show significant signatures of the solitons. For example, the probabilities which are indicative of the infective behaviour of the burst states include $P(1|001, 100)$, $P(1|011, 110)$, $P(1|101)$, $P(1|111)$, $P(1|112, 211)$, $P(1|122, 221)$, and $P(1|133, 331)$. In all the above configurations, the variable at the central site i changes into a burst state at time $t+1$, after being infected by a neighbouring burst state at time t.

Features of the creation, propagation, and annihilation of solitons are seen in the following update rules. As discussed earlier, a small fraction of the burst states are seen to generate pairs of left- and right-moving solitons. This information is contained in the following probabilities: $P(2|001, 100)$, $P(2|011, 110)$, $P(2|101)$, $P(2|111)$, $P(2|112, 211)$, $P(2|133, 331)$, $P(2|113, 311)$. For instance, the update rule defined by the conditional probability $P(2|111)$ determines the probability of obtaining a solitonic state ($v_i^{t+1} = 2$) at site i at time $t + 1$, given that the sites $i - 1, i, i + 1$ exist in the burst state ($v_{i-1}^t, v_i^t, v_{i+1}^t = 1$) at time t. Figure 2a shows the probability $P(2|111)$ obtained at $\Omega = 0.0455$ for various values of the coupling strength ϵ. The probability has been calculated for a lattice of size 500 over 5000 time steps (after discarding 3000 transients), and has been averaged over 50 initial conditions. This soliton creation probability shows a prominent increase at $\epsilon = 0.9$, which implies that the burst states generate 'solitons' at $\epsilon > 0.9$. This is also the point at which spatiotemporal intermittency with synchronised laminar states bifurcates to spatiotemporal intermittency with travelling wave laminar states and solitons. The probabilities are further seen to die down to zero at $\epsilon = 0.96$. At this point, the synchronised solutions reappear in the phase diagram.

The probabilities which are indicative of the propagation of solitons through the lattice are as follows: $P(0|022, 220)$, $P(2|022, 220)$, $P(2|122, 221)$, $P(2|222)$, $P(2|233, 332)$, $P(2|223, 322)$, $P(2|232)$. Figure 2b shows the probability $P(0|220, 022)$ plotted for various values of ϵ at $\Omega = 0.0455$. The probability is non-zero for $0.9 < \epsilon < 0.96$. And finally, when the left- and right-moving solitons collide with each other, they either die down to the laminar state or give rise to turbulent bursts. Signatures of annihilation of the solitons are seen in the probabilities: $P(0|022, 220)$, $P(1|022, 220)$, $P(1|122, 221)$, $P(1|222)$, $P(1|223, 322)$, and $P(1|232)$. The probabilities $P(1|220, 022)$, and $P(1|222)$ are plotted in figure 2c. These probabilities are again seen to be non-zero for $0.9 < \epsilon < 0.96$. Hence, we see that the cellular automaton designed for spatiotemporal intermittency with travelling wave states describes the infection dynamics of the burst states as well as picks up the signatures of the creation, propagation, and the annihilation of the solitons.

4. Conclusions

In earlier studies, we saw that the transition from the spreading to non-spreading regime in the phase diagram of the coupled sine circle map lattice can be mapped onto a cellular automaton, whereby the cellular automaton undergoes a transition from a set of probabilistic cellular automata in the spreading regime to a deterministic cellular automaton in the non-spreading regime. In this paper, we show that a similar cellular automaton can be designed for spatiotemporal intermittency with travelling wave laminar states contaminated by solitons. This cellular automaton effectively picks up the key signatures of the solitons including their creation from the burst states, propagation through the lattice and their annihilation. Moreover, it detects the regions in the phase diagram, where the solitons and spatiotemporal intermittency with travelling waves are seen to exist. Hence, we see that the cellular automaton mapping, though a coarse-grained version of the coupled map lattice, can still recognise the salient features of the local dynamics, while filtering

out the intricate details. Therefore, cellular automata mappings can be used as a very useful tool in studying dynamics on spatially extended systems, as well as in other areas such as studies of critical behaviour of absorbing phase transitions [14,15], stock markets [16], traffic flows [17], and cell growth kinetics [18].

References

[1] G Pradhan and N Gupte, *Int. J. Bifurcation Chaos Appl. Sci. Eng.* **11**, 2501 (2001)
[2] N Chatterjee and N Gupte, *Phys. Rev.* **E53**, 4457 (1996)
[3] N Chatterjee and N Gupte, *Phys. Rev.* **E63**, 017202 (2000)
[4] T M Janaki, S Sinha and N Gupte, *Phy. Rev.* **E67**, 56218 (2003)
[5] Z Jabeen and N Gupte, *Phys. Rev.* **E72**, 16202 (2005)
[6] Z Jabeen and N Gupte, *Phys. Rev.* **E74**, 16210 (2006)
[7] A Sharma and N Gupte, *Phys. Rev.* **E66**, 036210 (2002)
[8] Z Jabeen and N Gupte, *Physica* **A384**, 59 (2007)
[9] H Chaté and P Manneville, *Physica* **D32**, 409 (1988)
[10] P Grassberger and T Schreiber, *Physica* **D50**, 177 (1991)
[11] T Bohr, M van Hecke, R Mikkelsen and M Ipsen, *Phys. Rev. Lett.* **86**, 5482 (2001)
[12] S Wolfram, *Rev. Mod. Phys.* **55**, 601 (1983)
[13] E Domany and W Kinzel, *Phys. Rev. Lett.* **53**, 311 (1984)
[14] G Odor, *Rev. Mod. Phys.* **76**, 663 (2004)
[15] G Ódor and N Menyhárd, *Phys. Rev.* **E73**, 036130 (2006)
[16] G Qiu, D Kandhai and P M A Sloot, *Phys. Rev.* **E75**, 046116 (2007)
[17] K Gao, R Jiang, Shou-Xin Hu, Bing-Hong Wang and Qing-Song Wu, *Phys. Rev.* **E76**, 026105 (2007)
[18] M Block, E Schöll and D Drasdo, *Phys. Rev. Lett.* **99**, 248101 (2007)